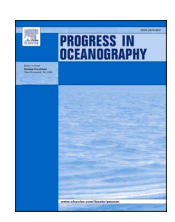
ELSEVIER

Contents lists available at ScienceDirect

Progress in Oceanography

journal homepage: www.elsevier.com/locate/pocean



Formation and circulation of newly ventilated winter water in the western Beaufort Sea

Peigen Lin^{a,b,*}, Robert S. Pickart^b, Thomas J. Weingartner^c, Harper L. Simmons^d, Motoyo Itoh^e, Takashi Kikuchi^e

- a School of Oceanography, Shanghai Jiao Tong University, Shanghai, China
- b Woods Hole Oceanographic Institution, Woods Hole, MA, USA
- ^c College of Fisheries and Ocean Sciences, University of Alaska, Fairbanks, USA
- ^d Applied Physics Laboratory, University of Washington, Seattle, WA, USA
- e Institute of Arctic Climate and Environment Research, Japan Agency for Marine-Earth Science and Technology, Yokosuka, Japan

ARTICLE INFO

Keywords: Newly Ventilated Winter Water Western Arctic Shelf Current Cold Halocline Water Ice production

ABSTRACT

Newly ventilated winter water (NVWW) is a cold, salty, nutrient-rich water mass that is critical for supporting the ecosystem of the western Arctic Ocean. In this study, NVWW formation is documented using timeseries from an 8-mooring array deployed from 2008 to 2009 across the shelf and slope in the western Beaufort Sea near 150°W. The saltiest (densest) class of the winter water (salinity > 32.6), which is able to ventilate the cold halocline in the interior Canada Basin, was only observed on the inner shelf from December to May. The reasons for this are three-fold: (1) In mid- to late-fall the water on the outer shelf is largely influenced by fresher water in the vicinity of the shelfbreak, limiting the density of the winter product there; (2) during winter the variance in ice cover is significantly higher on the inner shelf than the outer shelf, and this enhanced presence of leads and polynyas results in more re-freezing and hence formation of saltier winter water; and (3) the cross-shelf velocities during the cold months (December–May) were negligible at the array site. To better understand the ultimate fate of the salty NVWW, the components of the western Beaufort Sea boundary current system were quantified using the array data plus additional mooring data to the west. It is argued that the salty NVWW can be fluxed off the shelf due to the convergence of the westward-flowing current on the shelf and the eastward-flowing outflow from Barrow Canyon.

1. Introduction

In the western Arctic Ocean, the Bering Strait inflow of Pacific-origin water is the main source of heat, freshwater, and nutrients, which impact ice melt, halocline ventilation, and various aspects of the ecosystem (e.g., Steele et al., 2004; Woodgate et al., 2010). Previous studies have established the background circulation of the Pacific water in the western Arctic Ocean (e.g., Pickart et al, 2016; Lin et al., 2021). It flows northward along three main pathways on the Chukchi Sea shelf: a western pathway that flows to the northwest through Herald Canyon, a middle pathway flowing northward through Central Channel, and the Alaskan Coastal Current on the eastern shelf. A large amount of the Pacific water is fluxed off the shelf through Barrow Canyon and subsequently bifurcates, with the eastern branch feeding the Beaufort Shelf-break Jet and the western branch contributing to the Chukchi Slope

Current.

The Beaufort Shelfbreak Jet is present year-round but is subject to pronounced seasonality (Nikolopoulos et al., 2009; Brugler et al., 2014). It is strongest in summer when it is surface-intensified and accounts for 85 % of the annual transport. For the reminder of the year it is bottom-intensified with a small net eastward transport. Over the decade 2002–2012 the transport of the jet decreased by 77 % (Brugler et al., 2014), mostly due to strengthened easterly winds. As the jet flows eastward into the Canadian Beaufort Sea its transport diminishes (von Appen and Pickart, 2012; Lin et al., 2020). In addition to the primary circulation of the shelfbreak jet, secondary cross-slope flows arise throughout the year due to wind-driven upwelling and downwelling. This results in significant shelf-basin exchange of water, heat, and nutrients (Pickart et al. 2013; Lin et al., 2019; Foukal et al., 2019). The occurrence of upwelling/downwelling is not sensitive to ice cover as

E-mail address: plinwhoi@gmail.com (P. Lin).

^{*} Corresponding author.

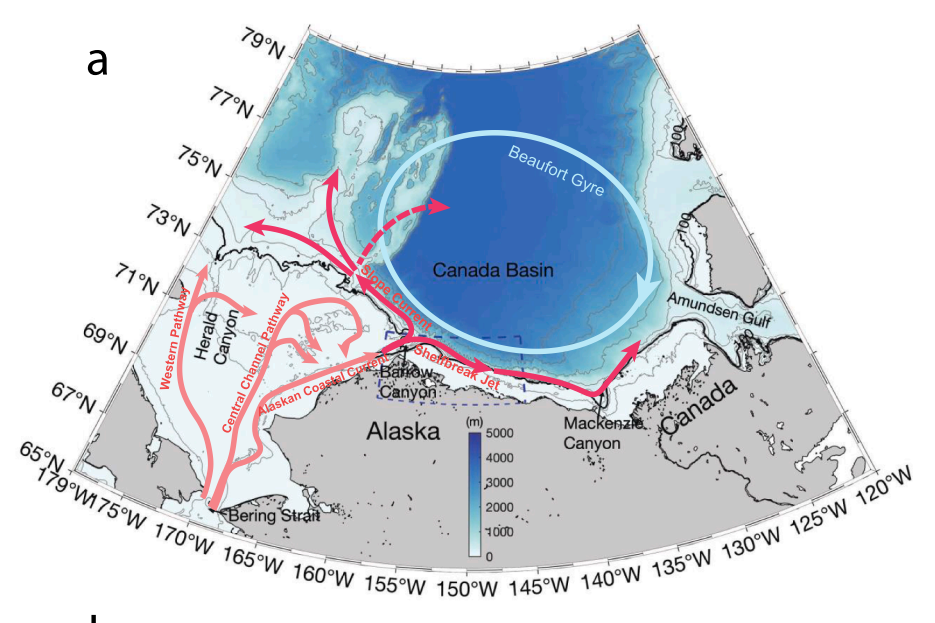
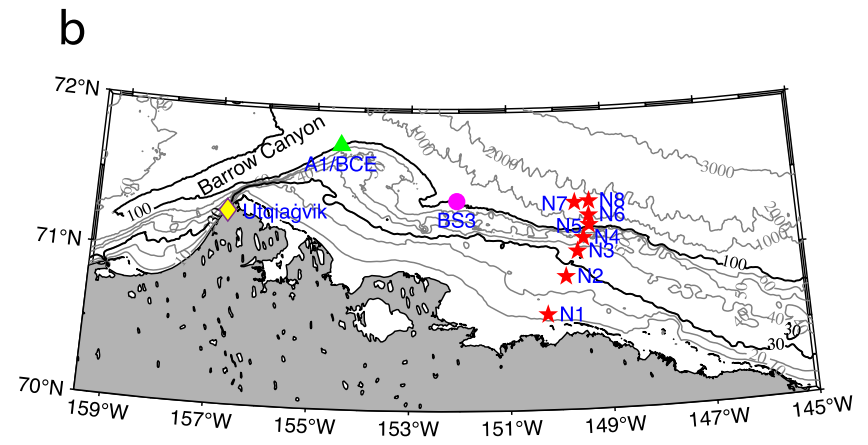


Fig. 1. (a) Schematic circulation of the western Arctic Ocean and geographic names. The pale red arrows represent the main pathways of the Pacific water on the Chukchi shelf. The Barrow Canyon outflow, Chukchi Slope Current and its downstream branches, and Beaufort Shelfbreak Jet are marked by the red arrows (the flow path denoted by the red dashed arrow is less certain). The schematic Beaufort Gyre is denoted by the light blue circle. The blue dashed box delimits the study region. (b) Enlarged view of the study region. Moorings N1–N8, BS3, A1/BCE, and the Utqiagʻvik meteorological station are marked by the red stars, magenta circle, green triangle, and yellow diamond, respectively. The bathymetry is from IBCAO v3.



long as the ice is mobile; however, its magnitude is intensified during periods of partial ice cover versus full ice cover (Schulze and Pickart, 2012).

The Pacific-origin water resident in the Chukchi and Beaufort Seas generally consists of four types: 1) Alaskan Coastal Water (ACW), the warmest and freshest of which is river run-off from Alaska (Weingartner et al., 2005); 2) Bering Summer Water (BSW), originating from the northern Bering Sea shelf during the warm months of the year (Steele et al., 2004); 3) Newly Ventilated Winter Water (NVWW), which is cold, salty water near the freezing point formed via convective overturning in the cold months of the year (Weingartner et al., 1998; Itoh et al., 2012; Pacini et al., 2019); and 4) Remnant Winter Water (RWW), which is NVWW that has been warmed by mixing and atmospheric heating (Gong and Pickart, 2016). In addition, a combination of sea-ice melt water and meteoric water (MWM) usually resides near the surface (Lin et al., 2020). Warm and salty Atlantic Water (AW) is found at depth beneath the Pacific water layer (Nikolopoulos et al., 2009).

All of these water masses are found in the western Beaufort Sea (e.g., Nikolopoulos et al., 2009; Lin et al., 2019). Using long-term mooring data, Lin et al. (2016) found that, within the Beaufort Shelfbreak Jet, the two winter waters are most commonly present: RWW is found throughout the year, accounting for over 50 % of the total water occurrence, while NVWW is present in all seasons except summer and accounts for the largest percentage in the water column in January-March. The two Pacific summer waters are mostly present in the warm months: BSW occurrence can approach 30 % in July and August,

while the warmer ACW is much less common (Lin et al., 2016).

The water mass occurrence and structure in the eastern Beaufort Sea is considerably different (Forest et al., 2015; Jackson et al., 2015; Lin et al., 2020). Pacific summer waters are rarely observed in the vicinity of Mackenzie Canyon, except for some sporadic occurrences of BSW on the shelf. Part of the reason for this is the fact that the shelfbreak jet spins down as it flows into the eastern Beaufort Sea (von Appen and Pickart, 2012). Furthermore, the Pacific summer waters residing in the upper layer are readily transformed along the pathway via mixing with ambient water and air-sea interaction (Steele et al., 2004; Timmermans et al., 2014). Lin et al. (2021a) argued that the local MWM originating from Mackenzie River, and/or ice melt, dominates the upper 50 m. This sets up a lateral barrier that prevents the Pacific summer waters from reaching the eastern Beaufort Sea. At these longitudes RWW occupies most of the middle layer over the slope, while NVWW was only observed on the shelf, with the highest percentages close to the coast.

NVWW has high concentrations of nutrients and trace metals due to interaction with the bottom sediments (Arrigo et al., 2017; Pacini et al., 2019; Dabrowski et al., 2022), and is also a primary source of ventilation of the cold halocline in the interior basin (Proshutinsky et al., 2019). It is well known that winter water is formed over the Bering and Chukchi shelves, particularly within polynyas and leads where the water readily refreezes (e.g., Weingartner et al., 1998; Woodgate et al., 2005; Itoh et al., 2013). The northeastern Chukchi shelf is a region of particularly frequent polynya formation in winter. The two main driving factors are wind-driven divergence of ice and sensible heat due to upwelling

Table 1
Information on the moorings used in the study.

N1						
	13.6	ADCP	1.5–11	0.5	1 hr	92.5
		(RDI Workhorse 600 kHz)				
		MicroCAT	13	-	1 hr	
		(SBE16+)				
N2	28	ADCP	3.9-25.4	0.55	1 hr	105.9
		(RDI Workhorse 600 kHz)				
		MicroCAT	27	_	1 hr	
		(SBE16+)				
N3	34	ADCP	6.3-26.3	4	1 hr	118.3
		(RDI Workhorse 300 kHz)				
		MicroCAT	32.9	_	15 min	
		(SBE57)				
		CWP (WHOI)	0.25-33.75	0.5	1 day	
N4	46	ADCP	9–37	4	1 hr	118.5
		(RDI Workhorse 300 kHz)				
		MicroCAT	43.7	_	15 min	
		(SBE57)				
		CWP (WHOI)	8.75-44.75	0.5	1 day	
N5	251	ADCP	19–209	12	1 hr	90.9
		(RDI Longranger 150 kHz)				
		MicroCAT	228	_	15 min	
		(SBE57)				
		CWP (WHOI)	0.25-39.25	0.5	1 day	
		CMP	46–224	2	6 hr	
		(WHOI)				
N6	1288	ADCP	6-62	4	1 hr	92.5
		(RDI Workhorse 300 kHz)				
		MicroCAT	69.6	_	5 min	
		(SBE37)				
		MMP (McLane Research Laboratories)	100-586	2	3 hr	
N7	1703	ADCP	7–63	4	1 hr	103.9
		(RDI Workhorse 300 kHz)				
		MicroCAT	69.9	_	5 min	
		(SBE37)				
		MMP (McLane Research Laboratories)	113-583	1	3 hr	
N8	1858	ADCP	8.5–100.5	4	1 hr	90.25
110	1000	(RDI Workhorse 300 kHz)	0.0 100.0	·		30.20
		MicroCAT (SBE37)	112	_	5 min	
BS3	147	ADCP	11.2–111.2	5	1 hr	125
_50	- **	(RDI Longranger 150 kHz)		-		
		MMP (McLane Research Laboratories)	54–120	2	6 hr	
A1	100	ADCP	3.2–79.2	1	0.5 hr	56
111	100	(RDI Workhorse 300 kHz)	J.E / J.E	-	J.J III	
BCE	107	ADCP	9.2–73.2	4	1 hr	
200	101	(RDI Workhorse 300 kHz)	3.2 7 3.2	•		

(Hirano et al., 2016). In particular, the strong northeasterly winds induce offshore Ekman transport in the surface layer that opens up the water in the coastal region. On the other hand, the northeasterly winds can also reverse the flow in Barrow Canyon and bring water from the basin onto the Chukchi shelf (Lin et al., 2021b; Ovall et al., 2021). Using mooring data, Li et al. (2022) determined that warm AW can occasionally be upwelled onto the shelf (10 % of upwelling events), which can melt pack ice. This is consistent with previous observational and modeling studies (e.g., Ladd et al., 2016; Hirano et al., 2018). Polynya induced winter water formation has also been documented on the eastern Beaufort Sea shelf (Lin et al., 2021a; Jackson et al., 2015).

It is believed that a large amount of the winter water formed on the Bering and Chukchi shelves eventually enters the halocline in the Canada Basin (Proshutinsky et al., 2019). As noted above, Pacific-origin waters are transported northward through Barrow Canyon, which feed both the westward-flowing Chukchi Slope Current and the eastward-flowing Beaufort Shelfbreak Jet. Some of the water from the canyon also enters the basin directly via turbulent processes (Spall et al., 2008; MacKinnon, 2021). The NVWW flowing eastward in the Beaufort Shelfbreak Jet can subsequently be fluxed offshore to the basin during downwelling events (Jackson et al., 2015; Foukal et al., 2019; Lin et al., 2021a).

To date there has been limited work addressing the formation and

spreading of NVWW on the western Beaufort shelf, inshore of the shelfbreak jet. While evidence of convective overturning and NVWW formation exists in this region (Dabrowski et al., 2022), many questions remain, such as: How common is this process? What are the atmospheric conditions under which it occurs? What portion of the shelf is subject to winter water formation? What is the fate of the dense water? To address some of these questions, in this study we use data from a year-long mooring array that was deployed across the shelf and slope in the western Beaufort Sea from 2008 to 2009. This enables us to document the seasonal evolution of winter water formation across the shelf in the western Beaufort Sea for the first time and address its associated circulation.

2. Data and methods

2.1. Mooring data

A year-long mooring array was maintained across the shelf and slope in the western Beaufort Sea from September 2008 to August 2009 (Fig. 1). It consisted of four tripods on the shelf and a tall mooring just seaward of the shelfbreak as a part of National Ocean Partnership Program (NOPP) entitled "Circulation, cross-shelf exchange, sea ice, and marine mammal habitats on the Alaskan Beaufort Sea shelf", and three

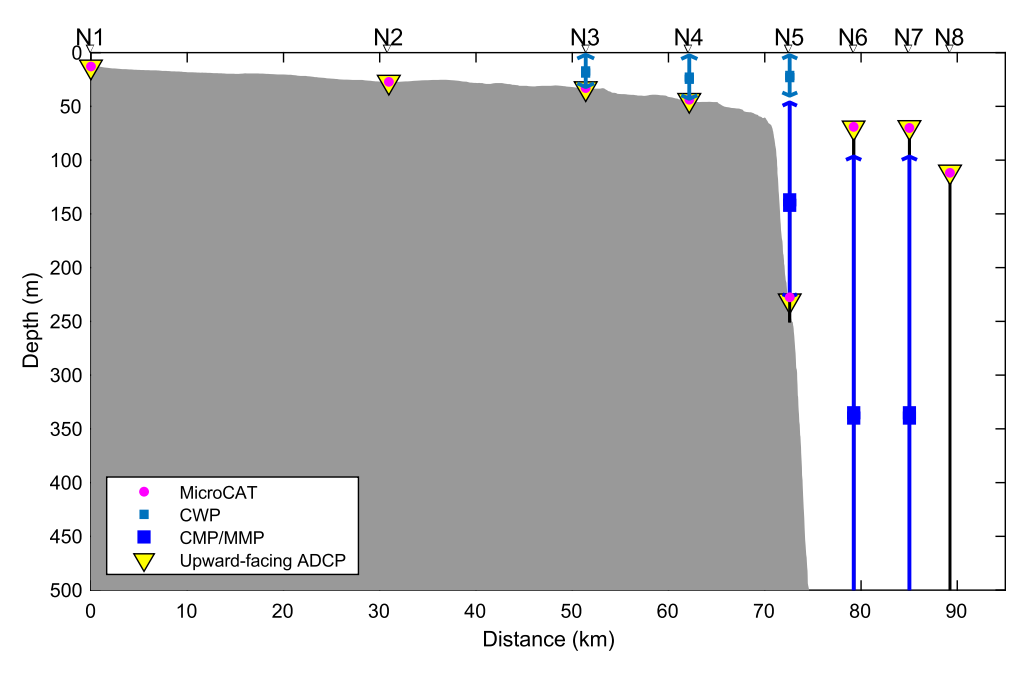


Fig. 2. Configuration of the NOPP/ICORTAS mooring array, N1–N8, in the cross-stream plane. The legend shows the instruments used on the moorings and their profiling ranges: MicroCAT; Coastal Winched Profiler (CWP); Coastal Moored Profiler (CMP); McLane Moored Profiler (MMP); and acoustic Doppler current profiler (ADCP). The bottom topography was obtained using an echosounder on a REMUS vehicle (inshore part of the section) and on a research vessel (offshore part of the section).

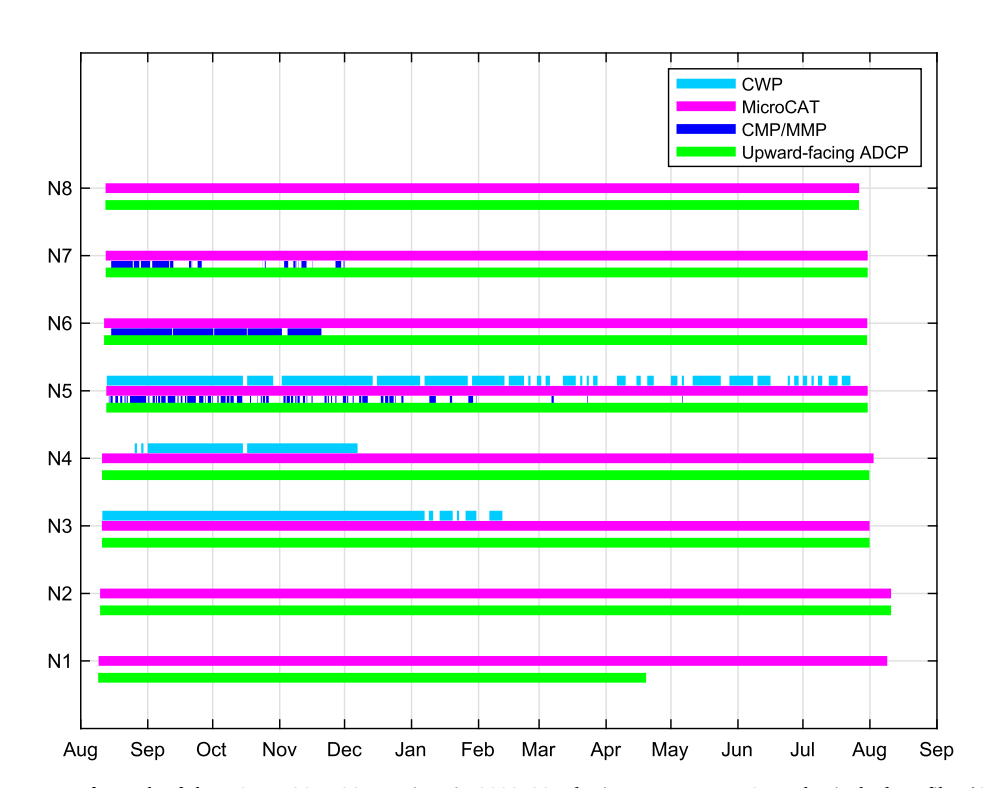


Fig. 3. Temporal data coverage for each of the NOPP/ICORTAS moorings in 2008–09. The instruments are: Coastal Winched Profiler (CWP), MicroCAT, Coastal Moored Profiler (CMP)/McLane Moored Profiler (MMP), and acoustic Doppler current profiler (ADCP), which are denoted by the bars in light blue, magenta, dark blue, and green, respectively (see the legend).

tall moorings on the continental slope as part of the program entitled "Ice Covered Response to Atmospheric Storms" (ICORTAS, Martini et al., 2014). In the paper we refer to these 8 moorings as N1–N8 from onshore to offshore (Fig. 1b and Table 1).

The configuration of the array in the cross-stream plane is shown in Fig. 2. Point hydrographic measurements at all of the moorings were obtained by MicroCATs, which were placed near the bottom of the shelf/shelfbreak moorings N1–N5 and on the top float (70 or 110 m) of the slope moorings N6–N8. The sampling interval was 1 h at N1–N2, 15 min at N3–N5, and 5 min at N6–N8. A longer sampling interval was chosen

for the mooring on the inner shelf in case of a delayed recovery due to landfast ice cover. To be consistent, we made hourly timeseries of temperature and salinity at each mooring. Moorings N3–N7 also returned hydrographic profiles. The two outer shelf tripods N3–N4 were equipped with a Coastal Winched Profiler (CWP) consisting of a Falmouth Scientific Instruments conductivity-temperature depth (CTD) sensor suite mounted on a buoyant package attached to a tether. Once per day the package rose to the sea surface (or to the under-side of the ice), and, after its vertical motion stopped, a winch on the tripod pulled the package back down to a cradle where the data were transferred

inductively to a data logger. The bin size of these vertical profiles was 0.5 m. Mooring N5 near the shelfbreak had a CWP on the top float that measured the upper 40 m and a motorized Coastal Moored Profiler (CMP) containing a CTD that sampled the lower part of the water column with a bin size of 2 m. The hydrographic profiles at the slope moorings N6–N7 were obtained using a McLane Moored Profiler (MMP), sampling 8 times per day over the depth range from $\sim\!100$ to $\sim\!580$ m, with a bin size of 1–2 m. The hydrographic data from all the profilers were processed following the procedures described in Fratantoni et al. (2006). The accuracy of the temperature is estimated to be 0.002 °C, and for salinity 0.03, based on comparisons to the nearby MicroCAT sensors.

Velocity was measured hourly by upward-facing acoustic Doppler current profilers (ADCPs) with a vertical resolution spanning from 0.5 to 12 m (Fig. 2 and Table 1). The ADCPs were positioned at the bottom of moorings N1–N5 and on the top floats of moorings N6–N8. Below the top floats on N6 and N7, the MMPs returned vertical profiles of velocity every 3 h, measured by a Falmouth Scientific Instruments acoustic current meter.

There were significant data gaps in the array (Fig. 3). A tripod deployed near the 17-m isobath was not recovered. This is within the stamukhi zone and it is presumed that the tripod was destroyed by ice (the mooring was not given a name for the present study since it returned no data). Because the MMPs on the three slope moorings were programed to sample 8 times per day, it was expected that the batteries would only last about 3 months. Unfortunately, the MMP on N8 failed upon deployment, and the CMP at N5 near the shelfbreak only profiled sporadically (and stopped profiling completely after 6 months). The CWP on N3 (N4) stopped recording in February (December). These instruments were lost during winter, presumably snagged by uneven ice keels as the CWP approached the underside of the ice. Despite the overall poor data return of the CWPs, CMP, and MMPs, they recorded valuable profile data during part of the year, which will be used in future studies. For the present study we focus on the point measurements of hydrography. However, since N5 had no MicroCAT in the upper layer, we constructed a timeseries at 40 m by averaging the top bin of the CMP profiles and the bottom bin of the CWP profiles.

In addition to the NOPP/ICORTAS mooring data, we also use ADCP velocity data from three moorings deployed to the west of the array. Mooring BS3 was deployed during the same period (2008–2009) as part of the Arctic Observing Network. It was situated close to the shelfbreak, ~100 km to the west (magenta circle in Fig. 1b) and provided hourly profiles. Mooring A1 was part of a different NOPP project (Stafford et al., 2013) and was located on the eastern side of the mouth of Barrow Canyon, ~95 km to the west of BS3 (green triangle in Fig. 1b). It collected two profiles per hour over the two-year period 2008-2010, with a gap from 14 December 2008 to 30 July 2009. To extend the velocity timeseries at this location, we use data from mooring BCE (marked by the same green triangle in Fig. 1b) which has been maintained by the Japan Agency for Marine-Earth Science and Technology (JAMSTEC) for two decades as a part of their mooring array across the mouth of the Barrow Canyon. We use the velocity timeseries from 2011 to 2018 (there were no data from 2010 to 2011), which consisted of hourly profiles. Table 1 contains the detailed information for these three additional moorings. We also used the top bin of hydrographic data from the MMP on mooring BS3 for our analysis.

All of the velocities were de-tided using T_Tide harmonic analysis toolbox (Pawlowicz et al., 2002) and rotated to alongstream and cross-stream components at each mooring based on the orientation of the major axis of the variance ellipse at the site (the alongstream angles are listed in Table 1). For computing volume transports, we constructed a section of alongstream velocity for each hourly time step. For the three months of missing data at N1, since the velocity is weak and stable when ice covered, we extended the data to May with the mean velocity from January to April, and linearly extrapolated the velocity to this inshore site for the months of June and July.

2.2. Reanalysis data

We use 10-m wind data for the period 2008–2018 from the ERA5 reanalysis provided by the European Center for Medium-Range Weather Forecasts (ECMWF, Hersbach, 2018) (https://www.ecmwf.int/en/forecasts/datasets/reanalysis-datasets/era5). This hourly atmospheric reanalysis product has a spatial resolution of 0.25° and has been widely used in previous studies of this region (e.g., Stabeno and McCabe, 2020; Li et al., 2020). For each NOPP/ICORTAS mooring, the wind timeseries at the closest data point was used. Following Nikolopoulos et al. (2009), the alongcoast wind in the western Beaufort Sea is taken to be 105°T. Positive values denote westerly winds.

We also used the 2-m air temperature product from ERA5 for computing the ice production, discussed below.

2.3. Meteorological data

To better reflect the wind in the vicinity of Barrow Canyon, we use the 10-m wind data obtained from the weather station at Utqiagvik, Alaska (the yellow diamond in Fig. 1b, https://www.ncdc.noaa.gov/cdo-web/datasets/GHCND/stations/GHCND:USW00027502/detail).

The data were quality controlled and short gaps were interpolated over, as described in Pickart et al. (2013). We use the along-canyon wind (52°T, Pisareva et al., 2019), which is most highly correlated with the alongstream velocity in the canyon. Positive values are southwesterly winds (down-canyon).

2.4. Satellite ice concentration

The ice concentration product used in the study is the daily timeseries from the Advanced Microwave Scanning Radiometer for EOS (AMSR-E), from 2008 to 2009, provided by the Remote Sensing of Sea Ice Research Group at the University of Bremen (https://seaice.uni-bremen.de/). The spatial resolution is 3.125 km in the study region, which allows us to distinguish the ice conditions at the individual mooring sites. We computed the ice concentration within a $0.1^{\circ}\times0.1^{\circ}$ box around each mooring.

Ice production, represented by the thickness of newly-formed sea ice, H, is computed via an empirical formula from Maykut (1986), $H^2+5.1H=6.7\theta$, where $\theta=\int_o^t (T_f-T_a)dt$ is the integrated freezing-degree days, T_f is the freezing point of seawater, and T_a is the air temperature at 2 m above the sea surface. For the calculation, we interpolated the lower-resolution ERA5 2-m air temperature data onto the AMSR-E grid. Note that the relationship between ice thickness and integrated freezing-degree days becomes more tenuous as the ice becomes thicker, which may overestimate the ice formation (Maykut, 1986).

We also compute ice thickness based on theoretical considerations, following Cavalieri and Martin (1994). In particular, the ice thickness (H_i) is a function of the initial and final salinities $(S_0$ and $S_f)$ of the water and the salinity of the ice $(S_i=0.32S_0)$ at each mooring on the shelf via $H_i=\frac{n\rho_wD}{\rho_i}$, where ρ_w and ρ_i are the densities of sea water $(1\times 10^3~{\rm kg~m}^{-3})$ and ice $(0.92\times 10^3~{\rm kg~m}^{-3})$, respectively; D is the water column depth; and $n=\frac{S_f-S_0}{S_f-S_i}$ is the ratio of the mass of sea water and newly formed ice. We note that the hydrographic measurements are near the bottom, and we assume that the salty/dense water resulting from ice formation can readily reach the bottom on the shallow Beaufort shelf (e.g., Dabrowski et al., 2022).

3. Presence of NVWW on the shelf

As mentioned in the introduction, while the properties, distribution, and seasonality of the water masses in the western Beaufort Sea have been well documented within the shelfbreak jet, they are much less well studied inshore of this on the shelf. We begin our analysis by presenting

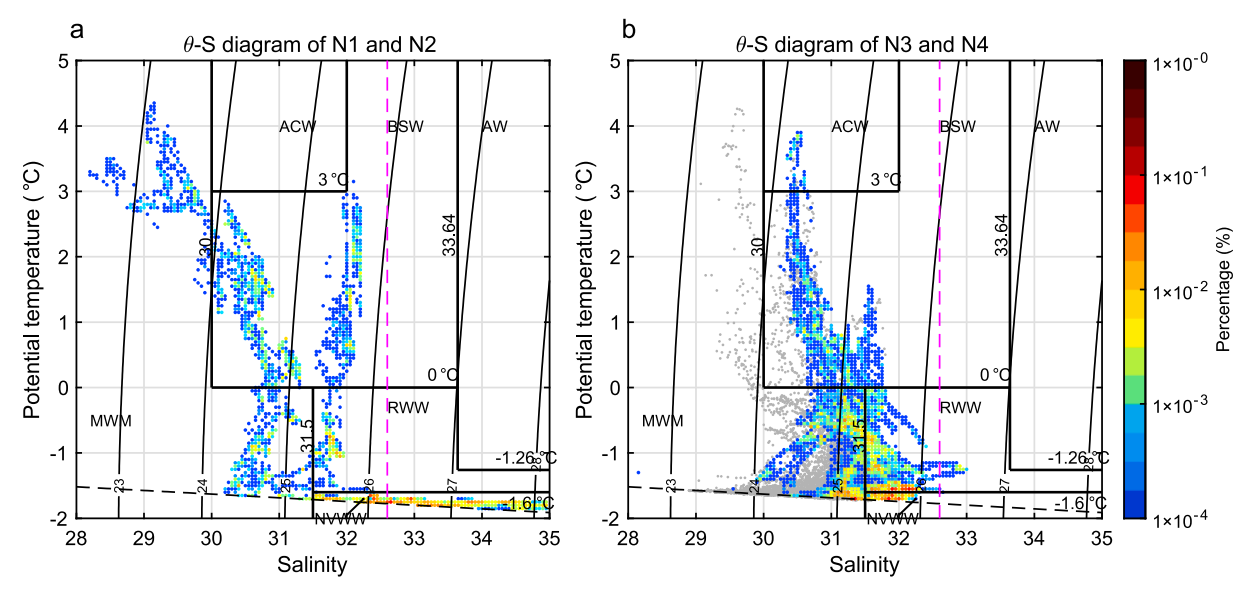


Fig. 4. Potential temperature-salinity (θ -S) diagram using near-bottom MicroCAT data from (a) the inner-shelf moorings, N1–N2, and (b) the outer-shelf moorings, N3–N4, for September 2008 to July 2009. The color coding indicates the percent occurrence. The magenta dashed line denotes salinity of 32.6, which represents the lower limit of CHW (see Table 2). The gray dots in (b) are the CMP data within the depth range of 30–40 m at N5. The black dashed line represents the freezing point. ACW = Alaskan Coastal Water; BSW = Bering Summer Water; NVWW = Newly Ventilated Winter Water; RWW = Remnant Winter Water; AW = Atlantic Water; and MWM = Melt Water/Meteoric Water.

Table 2 Potential temperature-salinity (θ -S) definitions of the water masses considered in the study (see also Pickart et al., 2019).

Alaskan Coastal Water (ACW)	$\theta > 3$ °C, S = 30–32		
Bering Summer Water (BSW)	$\theta =$ 0–3 °C, S = 30–33.64; $\theta >$ 3 °C, S =		
	32–33.64		
Remnant Winter Water (RWW)	$\theta = -1.6$ –0 °C, S = 31.5–33.64		
Newly Ventilated Winter Water	$\theta < -1.6~^{\circ}\text{C}, \text{S} > 31.5$		
(NVWW)			
Cold Halocline Water (CHW)	heta < -1.6 °C, S > 32.6		
Melt Water/Meteoric Water (MWM)	$\theta < 0$ °C, S = 30–31.5; S < 30		
Atlantic Water (AW)	$\theta > -1.26 ^{\circ}\text{C}.\ \text{S} > 33.64$		

percent occurrence potential temperature-salinity (θ -S) diagrams using the near-bottom data at the two inner-shelf moorings, N1 and N2 (Fig. 4a) and the two outer-shelf moorings, N3 and N4 (Fig. 4b). The definitions of each of the water masses considered in the study are contained in Table 2; these are the same as used in many previous studies of the region (e.g., Li et al., 2019; Pickart et al., 2019). On the inner shelf, one sees that all types of Pacific water were present except for the warm ACW. There was both warm, fresh MWM as well as relatively colder, saltier MWM. Notably, cold NVWW accounts for the largest occurrence, covering a large salinity range from 31.5 to \sim 35. There are three main differences on the outer shelf: 1) the warm and fresh MWM was no longer present; 2) a small amount of ACW was present (consistent with the water properties in a similar depth range at the upper-slope mooring N5, see the gray dots in Fig. 4b); and 3) the saltier portion of NVWW with salinity >32.6 was nearly absent. This salty/dense winter water ventilates the cold halocline in the Canada basin (Pickart, 2004). Hereafter, this salty NVWW is referred to as Cold Halocline Water (CHW) (Cavalieri and Martin, 1994).

These inner-to-outer shelf differences are elucidated in Hovmöller plots using the near-bottom measurements, shown in Fig. 5 along with the timeseries of ice concentration averaged over the shelf (moorings

N1-N4). The warm and fresh MWM was present on the inner shelf until mid-October, which is the time when the outflow from the nearby Colville River has essentially collapsed. This is followed by the presence of the relatively colder and saltier MWM for roughly two weeks. As the ice was freezing up in November, the water started cooling and remained cold for over 8 months until the ice melted. The cold water ($\theta < -1.6$ °C) appeared first at the inshore-most site N1 in mid-October, then about a month later at the next offshore site N2. At the two outer-shelf sites, N3 and N4, the cold water appeared even later (in December) and was present intermittently over much of the winter – in contrast to the innershelf where the cold water persisted without interruption. As the temperature decreased and finally reached the freezing point, the salinity of the inner-shelf water continually increased to the category of NVWW and ultimately to CHW (S > 32.6) starting in mid-January at N1 and mid-February at N2. These high values of salinity lasted for over four months. There was a small amount of RWW saltier than 32.6 present only at N3-N4 in December 2008, suggesting that such a signal did not originate from the inner-shelf but more likely was the result of upwelling that brought the salty RWW onshore (Fig. 5b, c).

Recall that winter water formation is largely attributed to sea ice production within polynyas and leads, which can be generated by wind forcing or/and heating (e.g., Hirano et al., 2016, 2018). To investigate the role of ice and the potential drivers of winter water formation, we focus on the cold months, December 2008–May 2009. The ice cover on the shelf fluctuated throughout this period (Fig. 6, black curve), conducive for winter water formation. With regard to the wind, we compared the timeseries of ice concentration with the occurrence of upwelling-favorable alongcoast winds which can induce Ekman divergence and form leads; however, no clear relationship was found.

Alternatively, one might expect that strong fluctuations of the alongcoast winds may be able to break up the pack ice. To investigate this, we computed the timeseries of standard deviation (SD) of the alongcoast wind on the shelf (i.e., the spatially averaged ERA5 wind in the vicinity of the N1–N4 moorings). In particular, for each time step the SD was computed using 5 data points before and after (11 data points in total). This was then compared to the timeseries of ice concentration on the shelf (i.e., the spatially averaged AMSR-E ice concentration in the vicinity of the N1–N4 moorings). The two timeseries are significantly correlated (Fig. 6, compare the red and black curves) with a maximum

¹ We note that the winter water masses identified by Jackson et al. (2015) on the eastern Beaufort shelf, the so-called Beaufort Sea Winter Water and Cold Shelf-water Intrusions, are contained within our definition of NVWW.

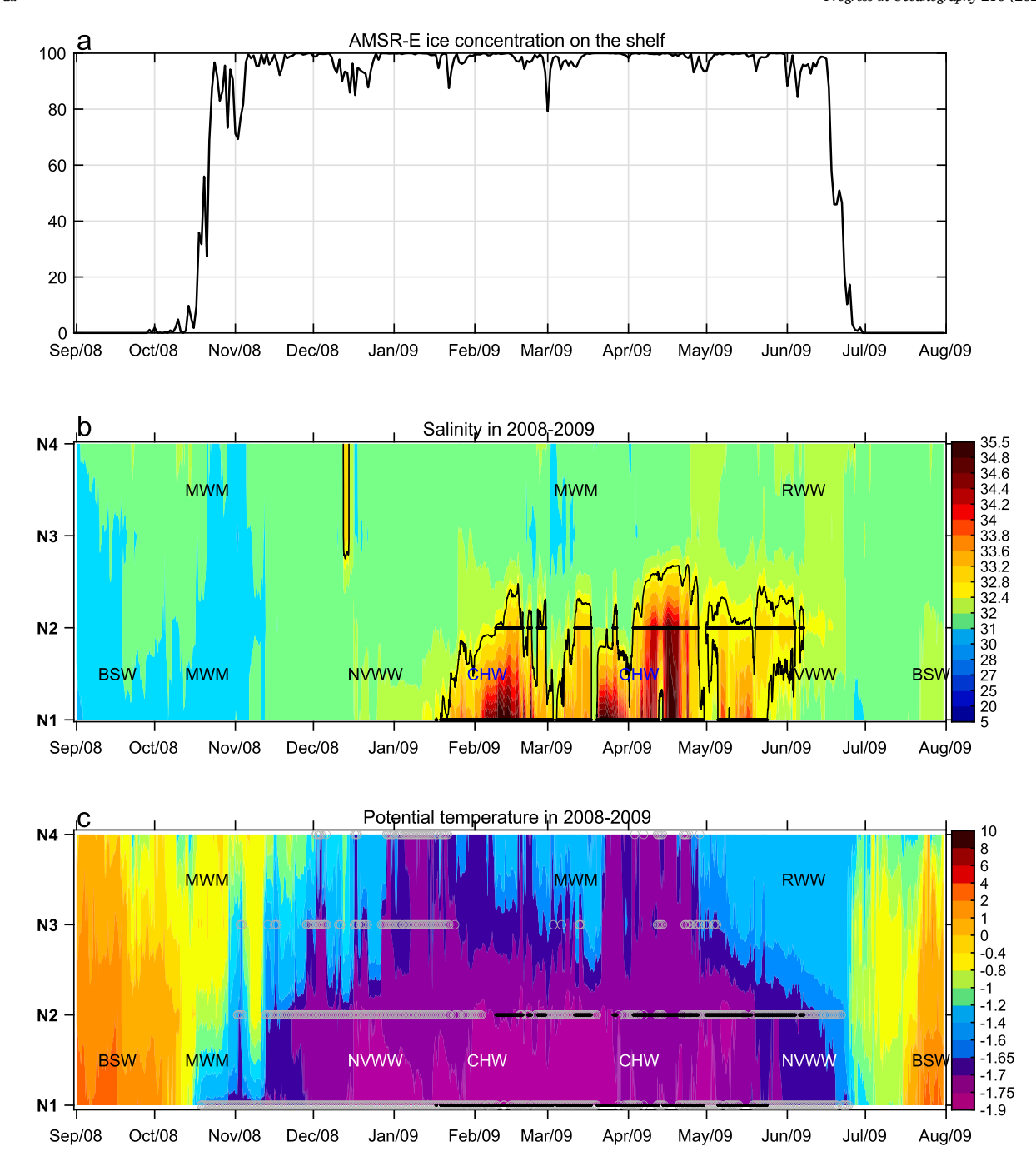


Fig. 5. (a) Timeseries of ice concentration from AMSR-E on the shelf (mean of N1-N4). The two lower panels are Hovmöller diagrams of (b) salinity and (c) potential temperature near the bottom of N1(17 m)-N4 (43.7 m), with the periods of cold halocline water (CHW) presence marked by the black dots. The black contour in (b) is the salinity of 32.6, the lower limit of CHW. Times when the temperature is near the freezing point in (c) at each mooring are marked by grey circles.

lag-correlation of R = 0.57 (p < 0.01) where the variance of the alongcoast wind leads changes in ice concentration by 3 days. At the same time, the currents are also influenced by the winds as long as the pack ice is mobile. As such, it is reasonable to believe that current fluctuations could open up the ice from beneath (e.g., Morales Maqueda et al., 2004). We constructed the analogous timeseries of the SD of the alongstream velocity on the shelf (averaged vertically in the water column and spatially between N1–N4). This also agrees well with changes in the ice concentration, with a peak R = 0.71 (p < 0.01) when the velocity variance leads by 2 days. We did not consider heat-driven ice reduction since there was no warm water upwelled to the inner-shelf (in contrast to what frequently occurs on the Chukchi shelf). These results suggest that variations of the local wind and currents can open up leads

in the ice which in turn leads to the formation of winter water.

Is there a geographic difference in the ice condition that leads to the presence of CHW on the inner shelf but not the outer shelf? To investigate this, we computed the mean and SD of ice concentration over the broader study region for the cold months, using the high-resolution AMSR-E data (~3.125 km) (Fig. 7). One sees the relative low ice concentration within Barrow Canyon and adjacent to the Beaufort coast, as well as a filament of reduced concentration along the 30-m isobath (Fig. 7a). These relatively low ice concentration areas correspond with the areas of high variance of ice (compare Fig. 7a and 7b). Notably, the two inner shelf moorings N1–N2 are within regions of less ice cover/greater ice variance than moorings N3 and N4. Following the method of Maykut (1986), we computed the integrated ice production over the

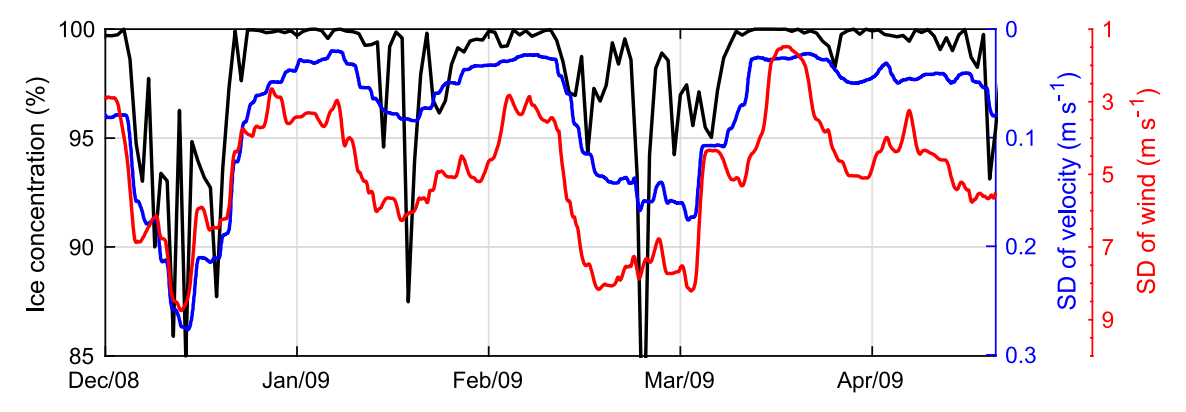


Fig. 6. Timeseries during the cold months of ice concentration spatially averaged over the vicinity of the shelf moorings N1–N4 from AMSR-E (black curve), standard deviation (SD) of alongstream ocean velocity (blue curve), and SD of alongcoast wind (red curve) on the shelf (mean of N1–N4). The ice concentration has been shifted forward by 3 days corresponding to the time lag of peak correlation with the alongcoast wind.

year-long time period, which is a direct indicator of the winter water formation (Fig. 7c). In line with the mean and SD of ice concentration, the ice production is higher at the inner shelf moorings. These results indicate that leads and polynyas are more frequently formed on the inner shelf, likely producing more NVWW as well as denser CHW.

As noted in Section 2.4, the empirical relationship for ice production employed by Maykut (1986) likely overestimates the true ice thickness as the layer increases. Applying the theoretical formula from Cavalieri and Martin (1994) (see Section 2.4 for details), the observed increase in salinity of NVWW at mooring N1 from 32 to ~34.5 requires ice formation of 1.5 m, while that at mooring N3 (salinity increase from 32 to 32.4) requires only 0.7 m ice production. This is consistent with the spatial pattern in Fig. 7c. We note that the ice production could also be overestimated due to the fact that our measurements are near the bottom; however, due to the shallow shelf, it is likely that during winter water formation the near-surface and near-bottom salinities closely track each other (e.g., Dabrowski et al., 2022).

These same cross-shelf differences in ice cover and variance are also found in the climatology (the mean and standard deviation of the annual-mean ice concentration over the 10-year period 2012–2022, not shown), suggesting that it is a common feature. The onshore-most mooring N1 is located close to the edge of the landfast ice zone on the Beaufort shelf, where the flow becomes unstable due to the large lateral velocity shear during the period of high ice variance in winter (Weingartner et al., 2017a). Regarding the leads along the 30-m isobath, we speculate that the widened shelf causes the currents that flow along the isobaths to diverge, which in turn induces the leads. This notion warrants further investigation, but is beyond the scope of our study.

As discussed above, the Hovmöller plots (Fig. 5b,c) demonstrate that, during the cold months of the year, the inner and outer shelves are largely isolated from each other hydrographically. To further quantify this, we computed the cross-correlation between the 7-day lowpassed salinity timeseries at the bottom of moorings N1-N4, at 45 m depth at mooring N5 (the only complete timeseries in the upper layer), and at 54 m depth at mooring BS3 to the west of the NOPP/ICORTAS array (the top bin of the MMP at mooring BS3). The selected depths at the latter two shelfbreak moorings are comparable to the shelf depth. The results are shown in Fig. 8. The two outer shelf moorings N3-N4 are highly correlated with each other ($R=0.80,\,p<0.01$), and also with N5 just seaward of the shelfbreak (R = 0.61 and 0.72, p < 0.01). This group is distinguished from the inner shelf moorings N1 and N2 which constitute their own separate group (R = 0.79, p < 0.01). This indicates that the water on the outer shelf is largely influenced by the water in the vicinity of the shelfbreak, unrelated to the inner shelf waters. Notably, in mid- to late-fall before the ice begins to form, the surface waters in the Beaufort Shelfbreak Jet and outer shelf are fresher than those inshore (evident from the hydrographic climatology used in Schulze and Pickart, 2012;

not shown). Such a fresh upper layer can prevent locally-formed NVWW from reaching the salinity limit of CHW.

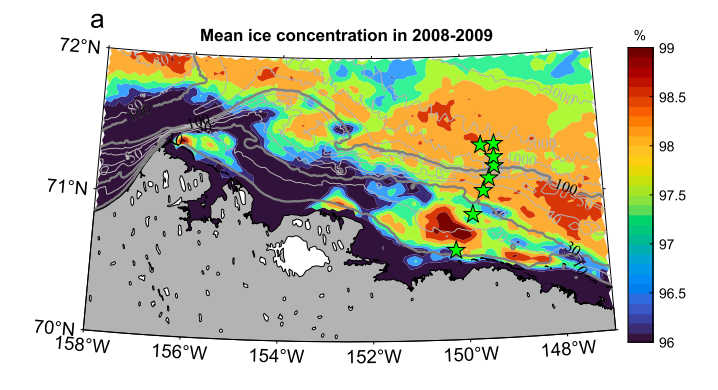
Fig. 8 reveals that the salinity at mooring BS3 is significantly correlated with mooring N2 on the inner shelf (R = 0.51, p < 0.01), seemingly at odds with the notion of isolation between the inner and outer shelves. However, as explained below in Section 4, west of the NOPP/ICORTAS array there is evidence that water from the inner shelf is fluxed offshore into the basin interior.

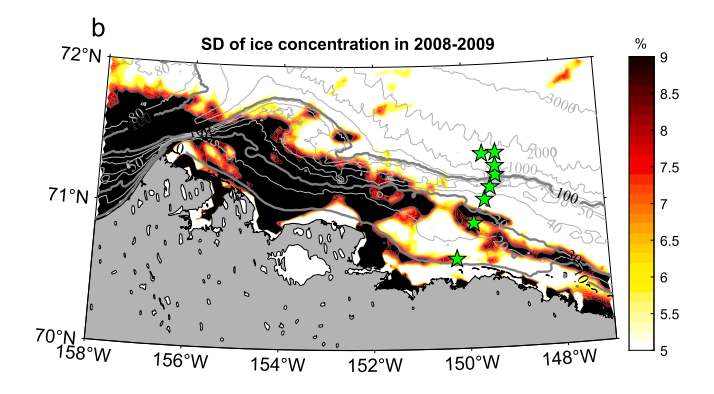
4. Circulation of the salty NVWW

4.1. Boundary current system

The above results imply that the formation of the salty NVWW – i.e., the CHW that ventilates the interior basin - only occurs on the inner shelf in the western Beaufort Sea, due to a combination of saltier resident water in fall and the enhanced occurrence of leads during winter. The next question is, what happens to this dense winter water after its formed, and is it able to escape the shelf? To address this, we first describe the boundary current system in the western Beaufort Sea using the NOPP/ICORTAS mooring data. The year-long mean verticallyaveraged velocity at each mooring is shown in Fig. 9a. Recall that the ADCP data at the three slope moorings (N6–N8) only cover the upper 60 m (see Table 1), while at N5, just seaward of the shelfbreak, the data extend to 200 m (we limited the averaging depth at N5 to 150 m to exclude the AW). This shows that the mean flow everywhere on the shelf (N1-N4) is directed to the west following the isobaths. Previous mooring studies have found that the flow within the landfast ice zone on the Beaufort shelf is typically close to zero in winter (Weingartner et al., 2017; Lin et al., 2020). Mooring N1, however, had a non-negligible velocity of ~0.02 m s⁻¹ westward during the cold months, indicating that it was mostly offshore of the immobile ice.

The vertical structure of the alongstream velocity is shown in Fig. 9b, revealing that the westward flow on the shelf is surface-intensified, extending from N1 to the outer shelf (between N4 and N5) with the peak velocity at N3. We refer to this as Beaufort Shelf Current. Even though the current advects different water masses, i.e., less dense water on the outer shelf and NVWW on the inner-shelf, we consider it a single coherent flow as all of the alongstream velocity records on the shelf are significantly correlated. Note that in the cold season, the presence of NVWW could form a density front that induces a westward flow. However, since the density front is weak and not stably present, the resulting flow is likely negligible. These are the first long-term moored observations spanning the full shelf in the western Beaufort Sea. Interestingly, in the eastern Beaufort Sea, just west of Mackenzie Canyon, there is also a westward-flowing shelf current (except immediately adjacent to the coast where the mean flow is directed eastward; Lin et al., 2020).





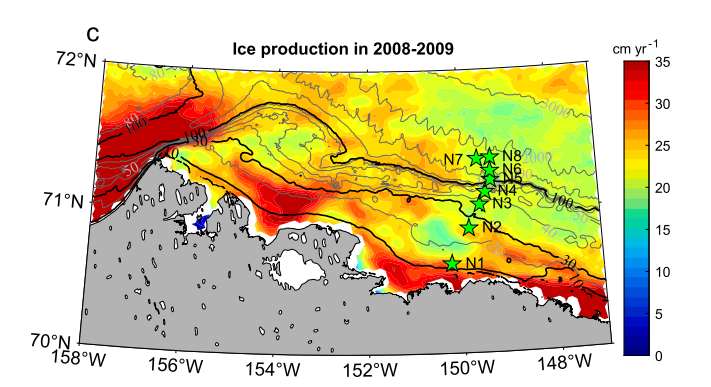


Fig. 7. Maps of (a) mean and (b) standard deviation of the AMSR-E ice concentration, and (c) ice production (cm ${\rm yr}^{-1}$), in the cold months (May-December) of 2008–2009. The bathymetry is from IBCAO v3. The 10-m, 30-m, and 100-m isobaths are highlighted. The NOPP/ICORTAS moorings are marked by the green stars.

Consistent with long-term mooring observations closer to Pt. Barrow (Nikolopoulos et al. 2009), the eastward-flowing Beaufort Shelfbreak Jet is also present at the NOPP/ICORTAS array. However, the steep topography of the upper slope at the NOPP/ICORTAS site makes it difficult to resolve the jet, and it was evident mainly at mooring N5 just seaward of the shelfbreak. In the mean, the jet is middepth-intensified (as it is farther to the west) with a maximum near 100 m. Seaward of this, the mean flow in the upper layer at N6-N8 is directed westward and surface-intensified. Such a velocity structure agrees with the westward flow that has been presented in previous observational and modeling studies of the continental slope of the western Beaufort and Chukchi Seas (Corlett and Pickart, 2017; Li et al., 2021; Leng et al., 2021). Hence, our observations indicate that the boundary current system in this part of the western Beaufort Sea includes three major components from onshore to offshore: the Beaufort Shelf Current, the Beaufort Shelfbreak Jet, and the (as yet unnamed) westward jet.

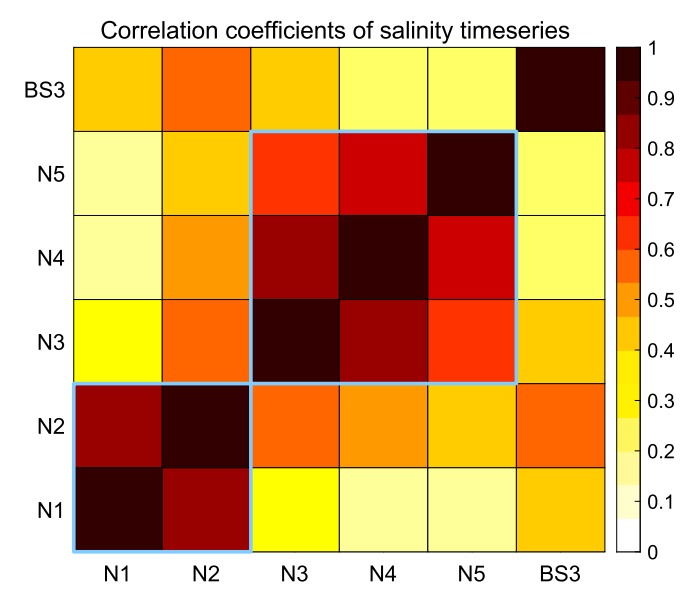
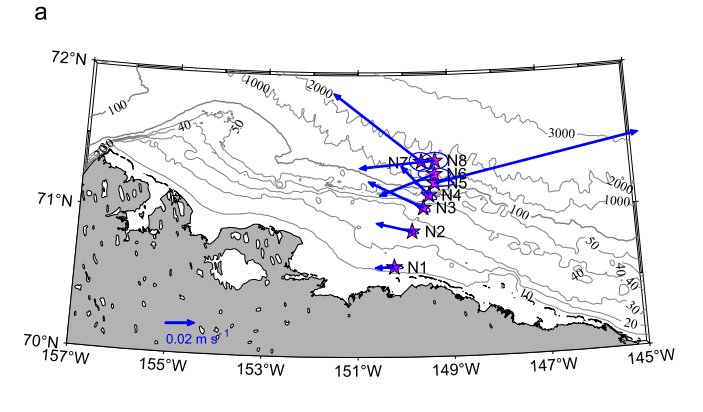


Fig. 8. Matrix of correlation coefficients of the salinity timeseries for moorings N1–N5 of the NOPP/ICORTAS array and mooring BS3 farther to the west. The two groups of moorings that are highly correlated with each other are outlined by the blue boxes.

To compute the corresponding volume transports, we made the following assumptions. The lateral range of the shelf current is taken to extend from mooring N1 to the location of the minimum of surface velocity in the mean section of alongstream velocity (see Fig. 9b). The vertical limit is down to the depth of the velocity corresponding to 10 % of the peak value of the mean shelf current. The transport of the westward jet over the continental slope was computed within the area of negative velocities located offshore of the shelf current. While this is clearly an underestimate, our results for the westward jet are consistent with the numerical study of Leng et al. (2021). Since the shelfbreak jet was only captured by a single mooring (N5), we are unable to estimate a volume transport. We thus used the transport of the jet computed for the same time period using mooring BS3 located ~100 km to the west of the NOPP/ICORTAS array. Brugler et al. (2014) developed an empirical proxy for estimating the transport of the jet using this mooring that was verified with data from an extensive 7-mooring array. The proxy has been employed in numerous subsequent studies (e.g., Lin et al., 2016).

Fig. 10 shows the monthly mean transport of each component of the boundary current system. One sees that the transports of the Beaufort Shelf Current were negative (westward) during most months of the deployment year, with a year-long mean transport of -0.05 ± 0.01 Sv. It had especially strong fluctuations in the warm months of 2008: peaking at -0.13 Sv in September, reversing to the east in October, and then recovering to the peak value. The transport varied much less in the following months (<0.1 Sv), and in April the transport was negligible. The transport of the Beaufort Shelfbreak Jet varied in phase to that of the shelf current, but with values on both sides of zero. Its year-long mean transport was 0.03 ± 0.02 Sv to the east. The transport of the slope jet presented here is the first observational estimate for this current. Interestingly, its transport varies in phase with the other two currents, but with a larger amplitude. It was directed westward in all months of the year except October and exceeded -0.2 Sv in September, November, March, and June. The year-long mean value is -0.12 ± 0.04 Sv, which is nearly identical to the -0.13 Sv determined from the numerical model study of Leng et al. (2021).

It has been demonstrated that the transport of the shelfbreak jet in the western Beaufort Sea is very sensitive to the alongcoast wind (e.g., Nikolopoulos et al., 2009). It is of interest to diagnose the effects of wind forcing on the other two components of the boundary current system. We constructed the monthly mean timeseries of alongcoast wind (black



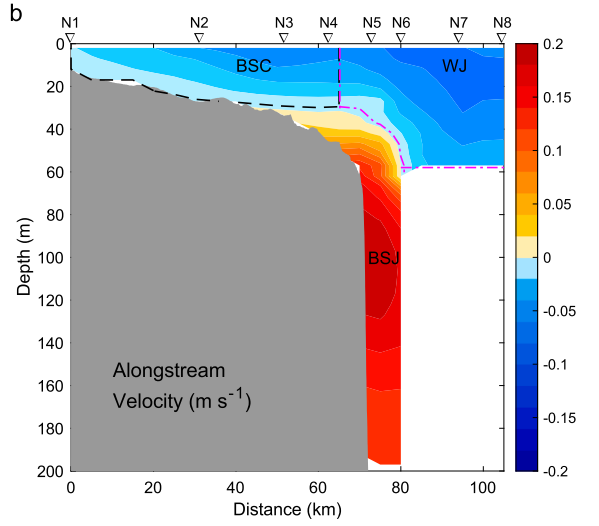


Fig. 9. (a) Mean vertically-averaged velocity vectors at the NOPP/ICORTAS array over the year of the deployment, with the standard error ellipses. The depth range for averaging is the full water column on the shelf, the upper 150 m at mooring N5, and the upper 60 m for moorings N6–N8. The magenta stars mark the mooring locations. The bathymetry data is from IBCAO v3, and the 100-m isobath is highlighted by the thick contour. (b) Vertical section of yearlong mean alongstream velocity. The dashed black curve delimits the extent of the Beaufort Shelf Current, defined as the sectional area ranging laterally from the location of N1 to the distance of the minimum surface velocity (between N4 and N5), and vertically bounded by the contour of the velocity corresponding to 10 % of the peak velocity of the current. The dashed magenta curve delimits the extent of the westward jet on the continental slope, which is defined as the region with negative velocities offshore of the shelf current. BSC: Beaufort Shelf Current; BSJ: Beaufort Shelfbreak Jet; WJ: the westward jet over the slope.

curve in Fig. 7). Not surprisingly, the alongcoast wind shows a similar seasonality to that of the shelfbreak jet transport. We computed the lagcorrelation between the two hourly timeseries. The peak correlation R = 0.48 (p < 0.01) is found when the shelfbreak jet lags the wind by 6 hrs. This time lag is consistent with that found in previous studies (e.g., Pickart et al., 2009). The variation of the shelf current transport is also highly correlated with that of the alongcoast wind: the wind forcing is 3 hrs ahead of the response of the shelf current, with R = 0.67 (p < 0.01). Such a strong correlation with wind is also true of the shelf current in the eastern Beaufort Sea. Leng et al. (2021) argued that the simulated westward jet near the southern edge of the Beaufort Gyre is dynamically linked to the gyre, under the control of large-scale atmospheric forcing in particular the strength and location of the Beaufort High (Armitage et al., 2016; Regan et al., 2019). Here we see good agreement between the transport of the westward jet on the continental slope and the local alongcoast wind: the response of the jet lags the alongcoast wind by 15 hrs, with R=0.4 (p < 0.01). This indicates that the local wind plays an important role in the high-frequency variability of the westward jet.

4.2. Fate of the cold halocline water

As shown Fig. 5, the CHW remained on the inner shelf throughout the year without being fluxed to the outer shelf, due to the negligible crossstream velocity computed using the NOPP/ICORTAS mooring data (on the order of 10^{-3} m s⁻¹). We note that the predicted downslope gravity flow of the dense CHW, based on the ideas in Baines and Condie (1998), is also negligible due to the gentle slope of the Beaufort inner shelf. The water thus more likely follows the shelf current to the west. To address the circulation of the CHW, we also consider the outflow from the eastern side of Barrow Canyon which could impact the boundary currents in the western Beaufort Sea. Recall that all of these currents are strongly affected by the winds, including the Barrow Canyon outflow, which can reverse under strong northeasterly along-canyon winds (e.g., Weingartner et al., 2017b; Pickart et al., 2019; Pisareva et al., 2019). Using the 10-year timeseries from the moorings located on the eastern side of the mouth of the Barrow Canyon (Fig. 1b), for each wind speed bin of 1 m s⁻¹, ranging from -8 to 8 m s⁻¹, we computed the mean alongstream velocity in the upper 25 m (corresponding to the water depth of mooring N2) of the outflow (56°T) over the cold months of December to May (blue curve in Fig. 11, where the velocity response time of 3 hrs has been taken into account). In line with previous studies, the down-canyon velocity increases as the southwesterly wind becomes stronger. Note that the relationship is not linear: the current strengthens more readily when the winds are extremely strong (in either direction). The zero-crossing occurs at a wind speed of -3.5 m s^{-1} , less than the wind threshold (-5 m s^{-1}) at the head of the canyon (Li et al., 2022). We also calculated the transport of the Beaufort Shelf Current for the same set of bins of along-canyon wind speed over the cold months using the year-long NOPP/ICORTAS mooring data (red curve in Fig. 11). The shelf current responds similarly to the winds, with a zero-crossing of $0.5 \,\mathrm{m\,s^{-1}}$ (a comparable result is obtained using the local alongcoast wind, with a zero crossing of 0.2 m s⁻¹). This near-zero wind threshold suggests that the direction of the shelf current is almost entirely dictated by wind, consistent with the situation in the eastern Beaufort Sea (Lin et al., 2020).

We now consider three circulation regimes according to the different states of the currents: (1) the Barrow Canyon outflow is reversed towards the southwest and the Beaufort Shelf Current flows westward; (2) the canyon outflow is weakly northeastward and the shelf current is weakly westward; and (3) the canyon outflow is strongly northeastward and the shelf current is reversed to the east. The three regimes are associated with along-canyon winds of $<-3.5 \text{ m s}^{-1}$, $-3.5 \text{ to } 0.5 \text{ m s}^{-1}$, and $>0.5 \text{ m s}^{-1}$, accounting for roughly 32 %, 40 %, and 29 % of the time, respectively, over the 10-year period of the Barrow Canyon mooring data, and 19 %, 45 %, and 36 % of the time, respectively, over the 1-year period of the NOPP/ICORTAS mooring data.

For the three circulation regimes, we constructed composite maps of the upper-layer velocity (averaged over the top 25 m) at all of the moorings based on the wind speed ranges (Fig. 12). We note that the mean Beaufort Shelfbreak Jet is bottom-intensified in the cold months of the year, hence its eastward flow at mooring N5 during periods of westerly winds is not well represented by the upper layer velocity.

In Regime 1, the winds are strongly out of the northeast/east over the entire domain. The flow in Barrow Canyon is strongly up-canyon, and the Beaufort Shelf Current is intensified to the west, with the largest velocities on the outer shelf, similar in magnitude to the velocity of the westward jet. Under these conditions the CHW will be advected by the inner-part of the shelf current towards the Chukchi shelf. In Regime 2, under weak northeasterly winds, the flow in Barrow Canyon is restored to be down-canyon. As such, the eastern branch of the outflow now opposes the westward shelf current, which could lead to convergence of the two currents on the inner shelf somewhere between the mouth of the canyon and the NOPP/ICORTAS mooring location. This in turn could flux the winter water off the shelf and into the basin. Lastly, in Regime 3, when the winds are out of the west, the canyon outflow is greatly

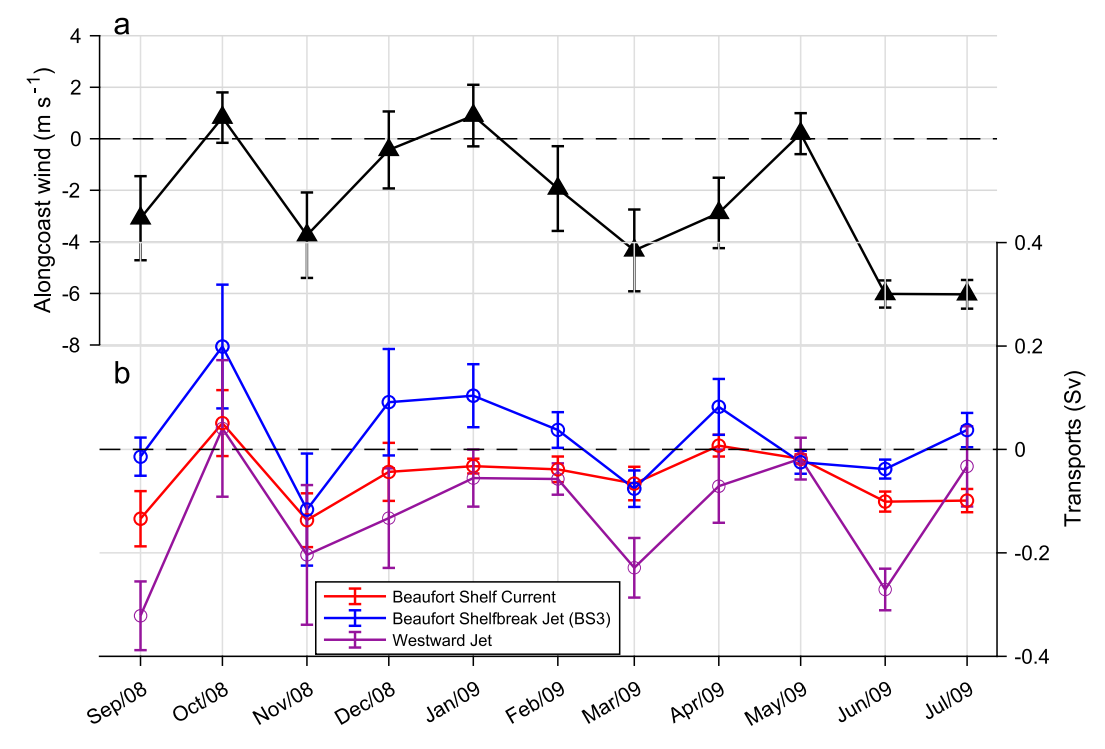


Fig. 10. (a) Monthly mean alongcoast wind (black curve). (b) Transport of the Beaufort Shelf Current (red curve), Beaufort Shelfbreak Jet (BS3, blue curve), and westward jet over the continental slope (purple curve). The errorbars are the standard errors.

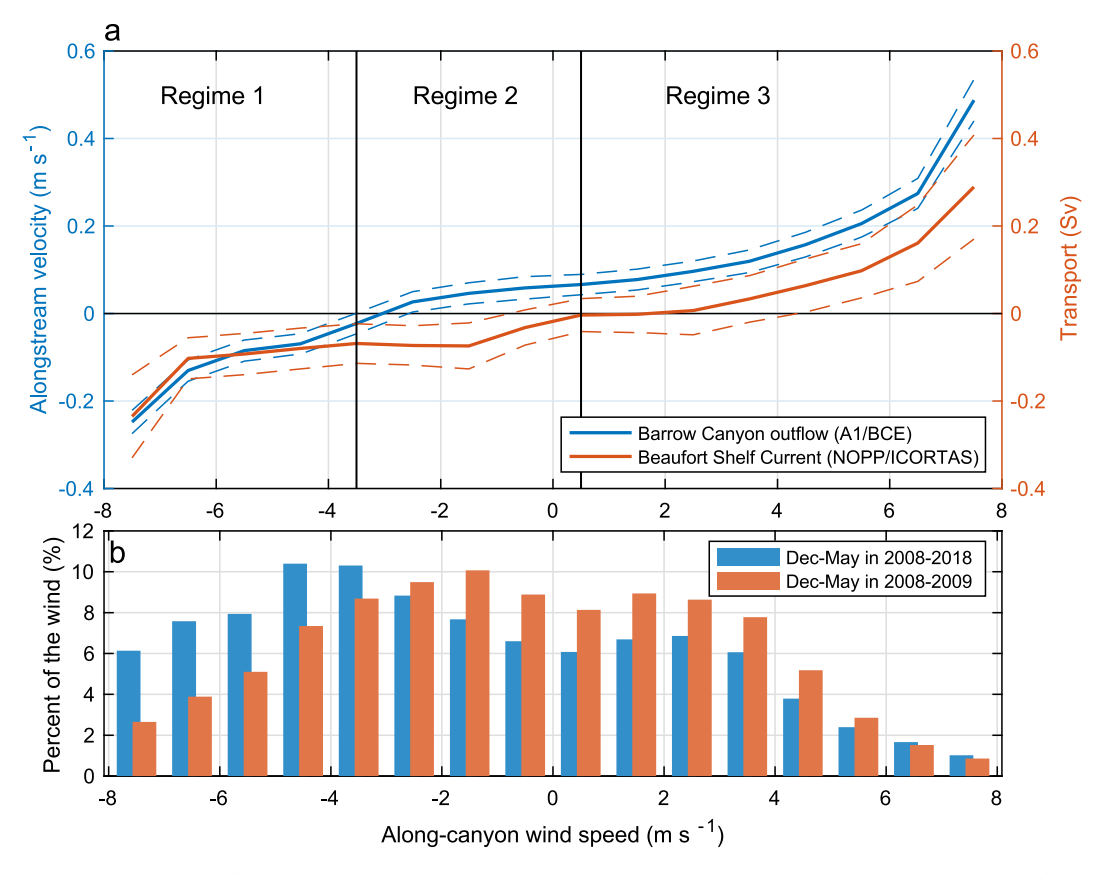
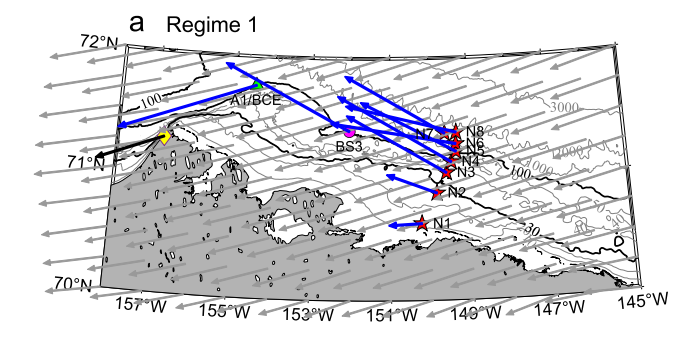
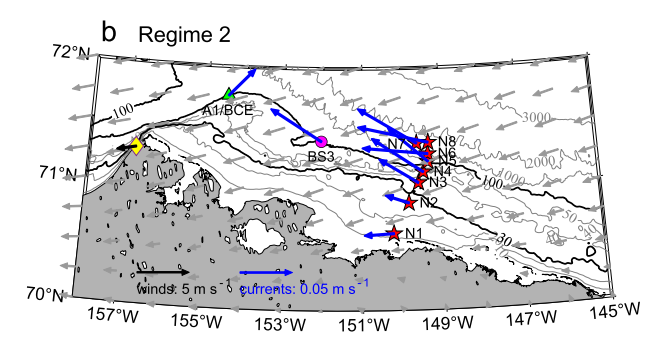


Fig. 11. (a) Alongstream velocity of the outflow on the eastern side of Barrow Canyon (blue curve) and volume transport of the Beaufort Shelf Current (red curve) as a function of along-canyon wind speed. Positive values are northeastward in the canyon and eastward along the shelf. Regime 1: the Barrow Canyon outflow is reversed towards the southwest and the Beaufort Shelf Current is westward; Regime 2: the canyon outflow is weakly northeastward and the shelf current is weakly westward; Regime 3: the canyon outflow is strongly northeastward and the shelf current is reversed to the east. The dashed lines are the standard errors. (b) Percentages of the wind data during the cold months for the 10-year period (blue bars) and 1-year period of the mooring array (red bars).





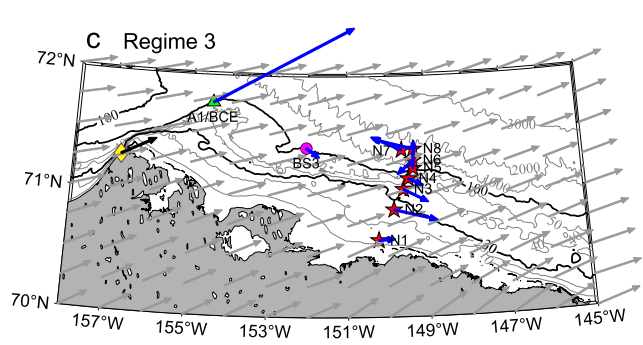


Fig. 12. Composite maps of the three circulation regimes defined in Fig. 11 during the cold months of December to May. The composites show the velocities in the upper 25 m (full depth at N1–N2), the 10-m ERA5 winds, and the winds at the Utqiagʻvik weather station (blue, grey, and black vectors, respectively). The bottom topography is from IBCAO v3.

intensified and the shelf current reverses to the east with the strongest flow at mooring N2 on the inner shelf. Thus, in Regimes 1 and 3 the CHW will be predominantly advected along the shelf, while in Regime 2 the water can be fluxed offshore. Notably, Regime 2 is the most common condition and close to the mean circulation state.

5. Conclusions

In this study we used multiple moorings along with ice and wind data to investigate the presence of Newly Ventilated Winter Water (NVWW) on the inner shelf of the western Beaufort Sea, including the factors leading to its formation and the potential fate of the water as influenced by the boundary current system. Comparing the hydrographic signatures across the NOPP/ICORTAS mooring line, we found that the densest NVWW, with salinity >32.6, was confined to the inner shelf. There are three reasons for this. First, in mid- to late-fall the water on the outer shelf is largely influenced by the fresher water in the vicinity of the shelfbreak, which limits the density of the winter product on this part of shelf. Second, during winter the variance of the ice cover is significantly higher on the inner shelf than the outer shelf. This enhanced presence of leads and polynyas means more re-freezing and hence formation of saltier winter water. Third, the cross-stream velocities during the cold

months of the year were negligible, meaning limited offshore spreading of the winter water at this location.

To understand the ultimate fate of the winter water, we first established the components of the boundary current system in the western Beaufort Sea, which consisted of the westward-flowing Beaufort Shelf Current, the eastward-flowing Beaufort Shelfbreak Jet, and surfaceintensified westward jet over the continental slope. On average, these currents flux -0.05 ± 0.01 Sv, 0.03 ± 0.02 Sv and -0.12 ± 0.04 Sv of water, respectively. They vary in phase with each other during the year in response to the alongcoast wind. We established three main windcirculation regimes: (1) under strong northeasterly winds, the Beaufort Shelf Current is intensified and the Barrow Canyon outflow is reversed to flow up-canyon; (2) when the northeasterly winds are weak, the shelf current remains westward and the canyon outflow is re-established; and (3) when the winds are southwesterly, the shelf current is reversed to the east and the canyon outflow is greatly strengthened. Regime 2 is the most common circulation pattern and can be thought of as the background state. Under this condition, the winter water on the inner shelf is carried by the westward-flowing shelf current and is likely fluxed offshore due to the convergence between the shelf current and the eastward-flowing outflow from Barrow Canyon.

Our study has highlighted the presence of a dense class of NVWW on the western Beaufort shelf and the boundary current system that can potentially flux this water off the shelf where it will ventilate the cold halocline in the interior Canada Basin. Previous studies have documented a similar densification of winter water on the Chukchi shelf (e.g., Itoh et al., 2012; Pacini et al., 2019), which drains northward out of Barrow Canyon (e.g., Pickart et al., 2005). Presently, the relative contributions of this cold halocline water (CHW) emanating from the Chukchi shelf versus the Beaufort shelf is unknown. We note that if the CHW documented in our study is formed on the inner shelf over the entire Beaufort Sea, then the volume formed in a single winter would be approximately 1200 km³. If all of this water were ultimately fluxed into the interior, it would be approximately half the amount of the CHW that is fluxed off the Chukchi shelf via Barrow Canyon. Future work is required to determine the extent of winter water formation on the Beaufort shelf and its year-to-year variability.

Declaration of Competing Interest

The authors declare that they have no known competing financial interests or personal relationships that could have appeared to influence the work reported in this paper.

Data availability

Data will be made available on request.

Acknowledgements

The authors are indebted to the crew of the USCGC *Healy* for the successful deployment and recovery of the NOPP/ICORTAS array. We thank Andy Mahoney for the insightful suggestion on ice production estimation. The fieldwork was supported by the National Ocean Partnership Program (NOPP) grant N00014-07-1-1040. The ICORTAS moorings (N6–N8 here) were supported by ONR Award N00014-06-1-0728. S. Okkonen provided the data from mooring A1, which was funded by NOPP grant WHOI A100587. The analysis was supported by grant OPP-1733564 from the National Science Foundation; grant NA19OAR4320074 from the National Oceanic and Atmospheric Association; and the Shanghai Pujiang Program (22PJ1406400), Shanghai Frontiers Science Center of Polar Science (SCOPS).

References

- Armitage, T.W., Bacon, S., Ridout, A.L., Thomas, S.F., Aksenov, Y., Wingham, D.J., 2016.
 Arctic sea surface height variability and change from satellite radar altimetry and GRACE, 2003–2014. J. Geophys. Res. Oceans 121 (6), 4303–4322.
- Arrigo, K.R., Mills, M.M., van Dijken, Lowry, K.E., Pickart, R.S., Schlitzer, R., 2017. Late Spring Nitrate Distributions Beneath the Ice-Covered Northeastern Chukchi Shelf. J. Geophys. Res. Biogeosci 122 (9), 2409–2417.
- Baines, P.G., Condie, S., 1998. Observations and modelling of Antarctic downslope flows: a review. In: Jacobs, S.S., Weiss, R.F. (Eds.), Ocean, Ice, and Atmosphere: Interactions at the Antarctic Continental Margin, Antarct. Res. Ser., Vol. 75, AGU, Washington, D.C., pp. 29–49.
- Brugler, E.T., Pickart, R.S., Moore, G.W.K., Roberts, S., Weingartner, T.J., Statscewich, H., 2014. Seasonal to interannual variability of the Pacific water boundary current in the Beaufort Sea. Prog. Oceanogr. 127, 1–20. https://doi.org/ 10.1016/j.pocean.2014.05.002.
- Cavalieri, D.J., Martin, S., 1994. The contribution of Alaskan, Siberian, and Canadian coastal polynyas to the cold halocline layer of the Arctic Ocean. J. Geophys. Res. Oceans 99 (C9), 18343–18362.
- Corlett, W.B., Pickart, R.S., 2017. The Chukchi slope current. Prog. Oceanogr. 153, 50–65.
- Dabrowski, J.S., Pickart, R.S., Stockwell, D.A., Lin, P., Charette, M.A., 2022. Physical drivers of sediment-water interaction on the Beaufort Sea shelf. Deep Sea Res. Part I: Oceanogr. Res. Pap. 181, 103700.
- Forest, A., Osborne, P.D., Fortier, L., Sampei, M., Lowings, M.G., 2015. Physical forcings and intense shelf-slope fluxes of particulate matter in the halocline waters of the Canadian Beaufort Sea during winter. Cont. Shelf Res. 101, 1–21.
- Foukal, N.P., Pickart, R.S., Moore, G., Lin, P., 2019. Shelfbreak downwelling in the Alaskan Beaufort Sea. J. Geophys. Res. Oceans 124 (10), 7201–7225.
- Fratantoni, P.S., Zimmerman, S., Pickart, R.S., Swartz, M., 2006. Western Arctic shelf-basin interactions experiment: processing and calibration of moored profiler data from the Beaufort shelf edge mooring array. Woods Hole Oceanographic Institution Tech. Rep. WHOI-2006-15, 34 pp.
- Gong, D., Pickart, R.S., 2016. Early summer water mass transformation in the Eastern Chukchi Sea. Deep Sea Res. II 130, 43–55.
- Hersbach, H., 2018. Operational global reanalysis: progress, future directions and synergies with NWP. European Centre for Medium Range Weather Forecasts.
- Hirano, D., Fukamachi, Y., Watanabe, E., Ohshima, K.I., Iwamoto, K., Mahoney, A.R., Eicken, H., Simizu, D., Tamura, T., 2016. A wind-driven, hybrid latent and sensible heat coastal polynya off Barrow, Alaska. J. Geophys. Res. Oceans 121 (1), 980–997.
- Hirano, D., Fukamachi, Y., Ohshima, K.I., Watanabe, E., Mahoney, A.R., Eicken, H., Itoh, M., Simizu, D., Iwamoto, K., Jones, J., Takatsuka, T., Kikuchi, T., Tamura, T., 2018. Winter water formation in coastal polynyas of the eastern Chukchi shelf: Pacific and Atlantic influences. J. Geophys. Res. Oceans 123 (8), 5688–5705.
- Itoh, M., Shimada, K., Kamoshida, T., McLaughlin, F., Carmack, E., Nishino, S., 2012. Interannual variability of Pacific Winter Water inflow through Barrow Canyon from 2000 to 2006. J. Oceanogr. 68 (4), 575–592.
- Itoh, M., Nishino, S., Kawaguchi, Y., Kikuchi, T., 2013. Barrow Canyon volume, heat, and freshwater fluxes revealed by long-term mooring observations between 2000 and 2008. J. Geophys. Res. Oceans 118 (9), 4363–4379.
- Jackson, J.M., Melling, H., Lukovich, J.V., Fissel, D., Barber, D.G., 2015. Formation of winter water on the Canadian Beaufort shelf: New insight from observations during 2009–2011. J. Geophys. Res. Oceans 120 (6), 4090–4107.
- Ladd, C., Mordy, C., Salo, S., Stabeno, P., 2016. Winter water properties and the Chukchi Polynya. J. Geophys. Res. Oceans 121 (8), 5516–5534.
- Leng, H., Spall, M.A., Pickart, R.S., Lin, P., Bai, X., 2021. Origin and fate of the Chukchi slope current using a numerical model and in-situ data. J. Geophys. Res. Oceans 126 (5).
- Li, M., Pickart, R.S., Spall, M.A., Weingartner, T.J., Lin, P., Moore, G., Qi, Y., 2019. Circulation of the Chukchi Sea shelfbreak and slope from moored timeseries. Prog. Oceanogr. 172, 14–33. https://doi.org/10.1016/j.pocean.2019.01.002.
- Li, J., Pickart, R.S., Lin, P., Bahr, F., Arrigo, K.R., Juranek, L., Yang, X.Y., 2020. The Atlantic Water Boundary Current in the Chukchi Borderland and southern Canada Basin. J. Geophys. Res. Oceans 125 (8).
- Li, J., Lin, P., Pickart, R.S., Yang, X.-Y., 2021. Time dependent flow of Atlantic Water on the continental slope of the Beaufort Sea based on moorings. J. Geophys. Res. Oceans 126 (6)
- Li, S., Lin, P., Dou, T., Xiao, C., Itoh, M., Kikuchi, T., Qin, D., 2022. Upwelling of Atlantic Water in Barrow Canyon, Chukchi Sea. J. Geophys. Res. Oceans 127 (3)
- Lin, P., Pickart, R.S., Stafford, K.M., Moore, G., Torres, D.J., Bahr, F., Hu, J., 2016. Seasonal variation of the Beaufort shelfbreak jet and its relationship to Arctic cetacean occurrence. J. Geophys. Res. Oceans 121 (12), 8434–8454.
- Lin, P., Pickart, R.S., McRaven, L.T., Arrigo, K.R., Bahr, F., Lowry, K.E., Stockwell, D.A., Mordy, C.W., 2019a. Water mass evolution and circulation of the northeastern Chukchi Sea in summer: Implications for nutrient distributions. J. Geophys. Res. Oceans 127 (7), 4416–4432.
- Lin, P., Pickart, R.S., Moore, G., Spall, M.A., Hu, J., 2019b. Characteristics and dynamics of wind-driven upwelling in the Alaskan Beaufort Sea based on six years of mooring data. Deep Sea Res. Part II 162, 79–92.
- Lin, P., Pickart, R.S., Fissel, D., Ross, E.d., Kasper, J., Bahr, F., Torres, D.J., O'Brien, J., Borg, K., Melling, H., Wiese, F.K., 2020a. Circulation in the vicinity of Mackenzie Canyon from a year-long mooring array. Prog. Oceanogr. 187, 102396.
- Lin, P., Pickart, R.S., Jochumsen, K., Moore, G., Valdimarsson, H., Fristedt, T., Pratt, L.J., 2020b. Kinematic Structure and Dynamics of the Denmark Strait Overflow from Ship-Based Observations. J. Phys. Oceanogr. 50 (11), 3235–3251.

- Lin, P., Pickart, R.S., Fissel, D.B., Borg, K., Melling, H., Wiese, F.K., 2021a. On the nature of wind-forced upwelling and downwelling in Mackenzie Canyon, Beaufort Sea. Prog. Oceanogr. 198, 102674.
- Lin, P., Pickart, R.S., Våge, K., Li, J., 2021b. Fate of warm Pacific water in the Arctic basin. Geophys. Res. Lett. 48 (20).
- MacKinnon, J.A., et al., 2021. A warm jet in a cold ocean. Nature commun. 12 (1), 2418. https://doi.org/10.1038/s41467-021-22505-5.
- Martini, K.I., Simmons, H.L., Stoudt, C.A., Hutchings, J.K., 2014. Near-inertial internal waves and sea ice in the Beaufort Sea. J. Phys. Oceanogr. 44 (8), 2212–2234.
- Maykut, G.A., 1986. The surface heat and mass balance. In: The Geophysics of Sea Ice. Springer, pp. 395–463.
- Morales Maqueda, M., Willmott, A., Biggs, N., 2004. Polynya dynamics: A review of observations and modeling. Review. Geophy. 42 (1).
- Nikolopoulos, A., Pickart, R.S., Fratantoni, P.S., Shimada, K., Torres, D.J., Jones, E.P., 2009. The western Arctic boundary current at 152°W: Structure, variability, and transport. Deep Sea Research II 56 (17), 1164–1181. https://doi.org/10.1016/j. dsr2.2008.10.014.
- Ovall, B., Pickart, R.S., Lin, P., Stabeno, P., Weingartner, T., Itoh, M., Kikuchi, T., Dobbins, E., Bell, S., 2021. Ice, wind, and water: Synoptic-scale controls of circulation in the Chukchi Sea. Prog. Oceanogr. 199, 102707.
- Pacini, A., Moore, G.W.K., Pickart, R.S., Nobre, C., Bahr, F., Våge, K., Arrigo, K.R., 2019. Characteristics and transformation of Pacific winter water on the Chukchi Sea shelf in late spring. J. Geophys. Res. Oceans 124 (10), 7153–7177.
- Pawlowicz, R., Beardsley, B., Lentz, S., 2002. Classical tidal harmonic analysis including error estimates in MATLAB using T_TIDE. Comp. Geosci. 28 (8), 929–937.
- Pickart, R.S., Moore, G.W.K., Torres, D.J., Fratantoni, P.S., Goldsmith, R.A., Yang, J., 2009. Upwelling on the continental slope of the Alaskan Beaufort Sea: Storms, ice, and oceanographic response. J. Geophys. Res. 114 https://doi.org/10.1029/ 2008jc005009.
- Pickart, R.S., Spall, M.A., Mathis, J.T., 2013. Dynamics of upwelling in the Alaskan Beaufort Sea and associated shelf-basin fluxes. Deep Sea Res. I 76, 35–51. https://doi.org/10.1016/j.dsr.2013.01.007.
- Pickart, R.S., Moore, G., Mao, C., Bahr, F., Nobre, C., Weingartner, T.J., 2016. Circulation of winter water on the Chukchi shelf in early Summer. Deep Sea Res. Part II 130, 56-75
- Pickart, R.S., Nobre, C., Lin, P., Arrigo, K.R., Ashjian, C.J., Berchok, C., Cooper, L.W., Grebmeier, J.M., Hartwell, I., He, J., 2019. Seasonal to mesoscale variability of water masses and atmospheric conditions in Barrow Canyon, Chukchi Sea. Deep Sea Res. Part II. https://doi.org/10.1016/j.dsr2.2019.02.003.
- Pickart, R.S., 2004. Shelfbreak circulation in the Alaskan Beaufort Sea: Mean structure and variability. J. Geophys. Res. 109 (C4) https://doi.org/10.1029/2003jc001912.
- Pisareva, M.N., Pickart, R.S., Lin, P., Fratantoni, P.S., Weingartner, T.J., 2019. On the nature of wind-forced upwelling in Barrow Canyon. Deep Sea Res. Part II. https:// doi.org/10.1016/j.dsr2.2019.02.002.
- Proshutinsky, A., Krishfield, R., Toole, J.M., Timmermans, M.-L., Williams, W.,
 Zimmermann, S., Yamamoto-Kawai, M., Armitage, T.W.K., Dukhovskoy, D.,
 Golubeva, E., Manucharyan, G.E., Platov, G., Watanabe, E., Kikuchi, T., Nishino, S.,
 Itoh, M., Kang, S.-H., Cho, K.-H., Tateyama, K., Zhao, J., 2019. Analysis of the
 Beaufort Gyre freshwater content in 2003–2018. J. Geophys. Res. Oceans 124 (12),
 9658–9689.
- Regan, H.C., Lique, C., Armitage, T.W., 2019. The Beaufort Gyre extent, shape, and location between 2003 and 2014 from satellite observations. J. Geophys. Res. Oceans 124 (2), 844–862.
- Schulze, L.M., Pickart, R.S., 2012. Seasonal variation of upwelling in the Alaskan Beaufort Sea: Impact of sea ice cover. J. Geophys. Res. Oceans 117 (C06022). https://doi.org/10.1029/2012jc007985.
- Spall, M.A., Pickart, R.S., Fratantoni, P.S., Plueddemann, A.J., 2008. Western Arctic shelfbreak eddies: Formation and transport. J. Phys. Oceanogra. 38 (8), 1644–1668.
- Stabeno, P.J., McCabe, R.M., 2020. Vertical structure and temporal variability of currents over the Chukchi Sea continental slope. Deep Sea Res. Part II 177, 104805.
- Stafford, K.M., Okkonen, S.R., Clarke, J.T., 2013. Correlation of a strong Alaska Coastal Current with the presence of beluga whales *Delphinapterus leucas* near Barrow, Alaska. Mar. Ecol. Prog. Ser. 474, 287–297.
- Steele, M., Morison, J., Ermold, W., Rigor, I., Ortmeyer, M., Shimada, K., 2004. Circulation of summer Pacific halocline water in the Arctic Ocean. J. Geophys. Res. Oceans 109 (C2).
- Timmermans, M.-L., Proshutinsky, A., Golubeva, E., Jackson, J.M., Krishfield, R., McCall, M., Platov, G., Toole, J., Williams, W., Kikuchi, T., Nishino, S., 2014. Mechanisms of Pacific summer water variability in the Arctic's Central Canada Basin. J. Geophys. Res. Oceans 119 (11), 7523–7548.
- von Appen, W.-J., Pickart, R.S., 2012. Two configurations of the western Arctic shelfbreak current in summer. J. Phys. Oceanogr. 42 (3), 329–351.
- Weingartner, T.J., Cavalieri, D.J., Aagaard, K., Sasaki, Y., 1998. Circulation, dense water formation, and outflow on the northeast Chukchi shelf. J. Geophys. Res. Oceans 103 (C4), 7647–7661.
- Weingartner, T.J., Danielson, S.L., Potter, R.A., Trefry, J.H., Mahoney, A., Savoie, M., Irvine, C., Sousa, L., 2017a. Circulation and water properties in the landfast ice zone of the Alaskan Beaufort Sea. Cont. Shelf Res. 148, 185–198.
- Weingartner, T.J., Potter, R.A., Stoudt, C.A., Dobbins, E.L., Statscewich, H., Winsor, P.R., Mudge, T.D., Borg, K., 2017b. Transport and thermohaline variability in Barrow

Canyon on the northeastern Chukchi Sea Shelf, J. Geophys. Res. Oceans 122 (5), 3565–3585.

Woodgate, R.A., Aagaard, K., Weingartner, T.J., 2005. A year in the physical oceanography of the Chukchi Sea: Moored measurements from autumn 1990–1991, Deep Sea Research Part II. Top. Stud. Oceanogr. 52 (24–26), 3116–3149.

Woodgate, R.A., Weingartner, T., Lindsay, R., 2010. The 2007 Bering Strait oceanic heat flux and anomalous Arctic sea-ice retreat. Geophys. Res. Lett. 37 (1), n/a-n/a.